Magnetic and Transport Properties of the Magnetic Polaron: Application to Eu$_{1-x}$La$_x$B$_6$ System

Unjong Yu and B. I. Min

Department of Physics, Pohang University of Science and Technology, Pohang 790-784, Korea
(Received 8 September 2004; published 22 March 2005)

To understand the role of the magnetic polaron in magnetic and transport properties of Eu$_{1-x}$La$_x$B$_6$, we investigate the low carrier density ferromagnetic Kondo lattice model by using the Monte Carlo methods. We demonstrate that the magnetic-polaronic (MP) state with the insulating nature is realized in the phase-separated region in between the ferromagnetic and antiferromagnetic (AFM) states in the phase diagram. The insulating behaviors of EuB$_6$ just above T_C and of Eu$_{1-x}$La$_x$B$_6$ with $0.05 < x < 0.2$ are well explained by MP states in the paramagnetic and the AFM background, respectively. The Eu vacancy plays a crucial role in forming the bound magnetic polaron and so producing the resistivity peak in EuB$_6$. By applying the weak magnetic field, the AFM metallic ground state is destroyed into the MP state, but the metallic behavior is restored by the strong magnetic field, as is observed for Eu$_{1-x}$La$_x$B$_6$ with $0.2 < x < 0.3$.

The concept of the magnetic polaron, introduced a long time ago [1], has attracted renewed attention in connection with doped magnetic semiconductors [2], high T_C cuprates [3], and colossal magnetoresistance (CMR) materials [4]. Various experiments, such as neutron scattering and spin-flip Raman scattering, indicate the existence of a magnetic polaron in a diluted magnetic semiconductor (DMS) [5], doped perovskite manganites [6], and Eu-based compounds [7–9]. There have been attempts to explain the intriguing features of these materials based on the magnetic polaron model [10,11]. However, the understanding of the existence condition and transport properties of magnetic polarons is far from complete. Specifically, there has been no explicit demonstration of the magnetic polaron formation in connection with transport experiments. In this Letter, we have investigated magnetic and transport properties of the magnetic polaron and applied it to the La doped EuB$_6$ systems to understand their unusual magnetic and transport properties. This study will shed light on understanding the underlying physics of the metal-insulator transition (MIT) near the magnetic transition, which is frequently observed in various spintronic materials.

EuB$_6$ is a low carrier density ferromagnetic (FM) metal with $T_C \approx 15$ K. The MIT occurs concomitantly with the FM transition. The intimate correlation between the magnetism and the transport property is believed to originate from the strong exchange interaction between spins of charge carriers and local f electrons [7]. It shares many common features with the CMR manganites, such as the MIT synchronized with the FM transition, large negative magnetoresistance (MR), and the experimental evidence of magnetic polarons. Distinctly from manganites, however, the lattice effect is weak and the carrier density is very low in EuB$_6$. In this respect, EuB$_6$ is an ideal system for studying magnetic polarons. Based on the magnetic polaron model with small lattice effect, Chatterjee *et al.* [11] successfully explained the transport behavior of EuB$_6$, including the MIT and large negative MR near T_C.

On the other hand, the La doped EuB$_6$ system (Eu$_{1-x}$La$_x$B$_6$) exhibits quite anomalous magnetic and transport properties. For small La doping with $x < 0.03$, the system is a FM metal, but both the saturation magnetic moment and the FM transition temperature are reduced considerably with La doping [8,12]. More La doping with $0.05 < x < \sim 0.2$ induces the spin-glass-like insulating ground state [12,13]. This is surprising since LaB$_6$ is more metallic than EuB$_6$. Interestingly, the external magnetic field restores the FM metallic state with large negative MR at low temperature, which suggests that the insulating gap feature has a magnetic origin. For further doping of La up to $x = 0.3$, the system becomes metallic but now antiferromagnetic (AFM) [13]. This reentrant metallic phase is destroyed by applying the magnetic field but is revived again for the stronger magnetic field. These experimental findings certainly indicate that the La doping somehow introduces the AFM interaction to the EuB$_6$ system, but the underlying mechanism has not been clarified yet. Presumably, the variation of the carrier density with La doping would change the RKKY-type exchange interaction from FM to AFM.

In order to elucidate anomalous magnetic and transport properties of Eu$_{1-x}$La$_x$B$_6$ in terms of the magnetic polaron, we have employed the FM Kondo lattice model with the AFM interaction between local magnetic moments:

$$H = -t \sum_{\langle i,j \rangle \sigma} (c_{i\sigma}^\dagger c_{j\sigma} + \text{H.c.}) - J_H \sum_i \vec{\sigma}_i \cdot \vec{S}_i + J_{AF} \sum_{\langle i,j \rangle} \vec{S}_i \cdot \vec{S}_j$$
$$+ \sum_{i\sigma} \varepsilon_i c_{i\sigma}^\dagger c_{i\sigma}, \tag{1}$$

where $c_{i\sigma}^\dagger$ creates a charge carrier with spin σ at site i, and $\vec{\sigma}_i$ and $\vec{S}_i$ are spins of the carrier and local moments, respectively. t and J_H represent the hopping parameter and the Hund-type coupling between the carrier spin and local moments. t is used as an energy unit ($t = 1$), and we have assumed a very large J_H/t ratio as much as 20. The

J_{AF} term is included to consider the AFM interaction induced by La doping, effectively. The precise value of J_{AF} is not available, but it is reasonable to presuppose that J_{AF} is zero or very small for EuB_6 and increases with La doping. For local $\vec{S}_i$, the Ising-type spin is adopted ($S_z = \pm 1/2$). In the case of EuB_6, the local spin magnitude is $7/2$ coming from f electrons of Eu^{2+}, but the result is not sensitive to the spin size, as shown below. $\langle i, j \rangle$ runs over nearest-neighbor lattice pairs. The last term corresponds to the site-dependent impurity potential, which is included to consider the disorder effects on the magnetic and transport properties later in Fig. 3. The carrier-carrier interaction is neglected because we are interested in the dilute carrier limit. Furthermore, the large value of J_H acts as the on-site Hubbard repulsion reducing the probability of double occupancy.

To solve the above model Hamiltonian, we have performed the Monte Carlo simulation using the standard Metropolis algorithm [14] on the two-dimensional (2D) square lattice with the periodic boundary condition. The electronic energy has been calculated through the exact diagonalization method [15]. For low carrier density and low temperature cases, we have used the Davidson algorithm [16], which accelerates the calculation remarkably.

The phase diagram on a similar model with classical local spins has been reported previously [17]. It was found that there exists the phase-separated (PS) region near half filling ($n = 1$) even without the AFM interaction between local moments [18]. With the AFM interaction, the PS region expands and a new PS region appears at low carrier density. The PS region is characterized by the discontinuity in carrier density by varying the chemical potential μ at very low temperature. It means that a state with some specific carrier density is unstable so that there occurs the segregation into carrier-rich and carrier-poor regions. The physical nature and properties of the PS states, however, have not been addressed. In this study, we have scrutinized the PS region and proved that the PS region in the low carrier density limit is closely related to the magnetic-polaronic (MP) state.

Figure 1(a) shows the phase diagram we have obtained. The relations between the carrier density n and μ, which were used to produce the phase diagram, are presented in Figs. 1(b) and 1(c) for $J_{AF} = 0$ and $J_{AF} = 0.2$, respectively. The PS region appears for $n > 0.77$ when $J_{AF} = 0$, whereas two PS regions exist when $J_{AF} > 0$ on each side of the FM or the short-range incommensurate spin-density wave (SDW) phase. Despite different assumption of the local spin size, the present result is equivalent to that of Ref. [17]. Figure 1(d) presents the local spin configurations for ground states in the low density side. We have performed the simulation on the PS region with fixed carrier density. The simulation temperature was reduced very slowly and it was repeated many times with a different random number sequence. With increasing J_{AF}, the ground state is transformed from the FM to the AFM state, and in
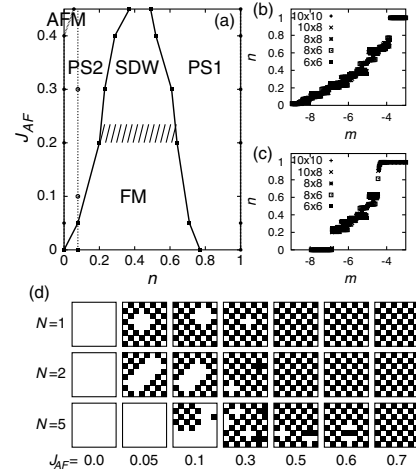
FIG. 1. (a) The low temperature ($T = 0.005$) phase diagram obtained for a 2D square lattice with size from 6×6 to 10×10 ($J_H/t = 20$). FM and SDW represent the ferromagnetic and incommensurate spin-density wave states, respectively, and PS1 and PS2, the phase-separated regions. For $n = 0$ and $n = 1$ (n, carrier density), the antiferromagnetic states appear. (b) n as a function of the chemical potential μ for $J_{AF} = 0$ with varying lattice size. The discontinuity at $\mu = -4$ indicates the PS region in the phase diagram. (c) The same as (b), but for $J_{AF} = 0.2$. (d) Snapshot of the local spin structure at $T = 0.005$ with varying carrier density and J_{AF}. Black and white rectangles represent sites with up and down local spins, respectively. The first row is for one carrier ($N = 1$) case in an 8×8 lattice ($n = 0.0156$). The second and third rows are for $N = 2$ ($n = 0.0313$) and $N = 5$ ($n = 0.0781$) cases, respectively. The parameters for $N = 5$ correspond to those along the vertical dotted line in (a). For $N = 1$, magnetic polaron features are clearly seen for $J_{AF} = 0.05$, 0.1, and 0.3, and similarly for $N = 2, 5$.

between the two states, that is, in the PS region, there appear FM clusters within the AFM background. We have obtained the same features for two and more carriers [$N = 2, 5$ in Fig. 1(d)]. They reveal the typical patterns of magnetic polarons, and thus the PS region can be regarded as the MP state, at least in the low carrier density region.

In Fig. 2, magnetic and transport properties are investigated at the low carrier density ($n = 0.0156$). The resistivity was calculated by using the Kubo formula and the f sum rule [19]. Finite broadening of 0.2 was assumed for delta functions to simulate broadening effects not considered in our idealized model. There are three regimes to be noted. (i) For the FM ground state with $J_{AF} = 0$, the magnetization increases upon cooling up to the full saturation. Finite magnetization of 0.1 at high temperature is due to the thermal fluctuation and becomes smaller for larger lattices. The susceptibility peak in the inset of Fig. 2(a) gives $T_C \sim 0.015$. In this case, the resistivity decreases monotonically with a small hump at the FM ordering [solid line in Fig. 2(b)]. (ii) For finite J_{AF}, the MP clustered state becomes the ground state and so the corresponding magnetization decreases. The resistivity decreases initially upon cooling but increases at low tem-
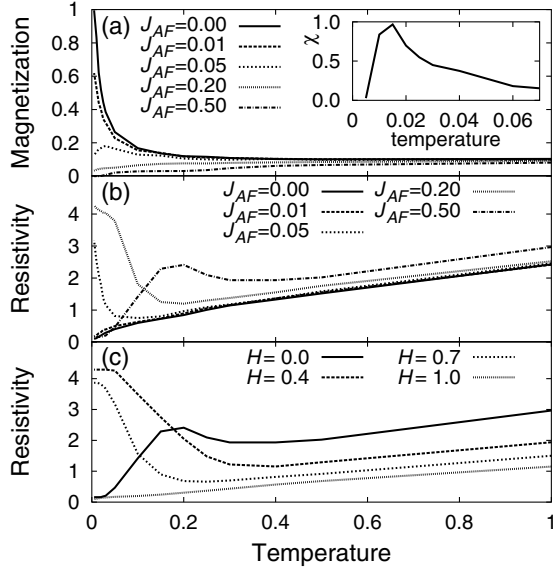
FIG. 2. (a) Magnetization and (b) resistivity as a function of temperature for $n = 0.0156$ with varying J_{AF}. Inset in (a) provides the magnetic susceptibility for $J_{AF} = 0$. (c) The resistivity versus temperature with varying applied magnetic field for $J_{AF} = 0.5$. Resistivity data are in arbitrary units.

perature, manifesting the insulating behavior. The insulating behavior at low temperature is common to all the MP clustered states. The FM clusters embedded in the AFM background induces the localization of charge carriers which gives rise to the insulating behavior due to the incoherent hopping of carriers. (iii) For the AFM ground state with $J_{AF} = 0.5$, the metallic behavior is restored at low temperature but with reduced conductivity as compared to the FM state [dot-dashed line in Fig. 2(b)]. In this case, there appears a peak in the temperature dependent resistivity reflecting an MIT. Figure 2(c) presents the effect of the external magnetic field on this AFM state. For the weak magnetic field, the AFM structure is broken and the system becomes insulating. The strong magnetic field, however, restores the metallic state without showing any peak in the resistivity. Accordingly, the MR at low temperature changes sign from positive to negative with increasing the magnetic field.

It is amusing to recognize the consistency between the present theoretical results and experimental data of $Eu_{1-x}La_xB_6$. The FM metallic state of EuB_6 can be associated with the small J_{AF} case in the above analysis, while the spin-glass-like insulating state for $0.05 < x < \sim 0.2$ can be associated with the MP clustered state and the AFM metallic state for $0.2 < x < 0.3$ with the large J_{AF} case, respectively. That is, the more La doping, the larger the AFM interaction. Then most of the anomalous transport behaviors in $Eu_{1-x}La_xB_6$ are understandable.

The only discrepancy is the insulating behavior observed for some region above T_C for $x = 0$. According to our result for small J_{AF}, the resistivity decreases monotonically upon cooling. It is likely that the absence of an

insulating region for $J_{AF} = 0$ is inherent in the model of Eq. (1). Then some other source of the localization mechanism needs to be invoked to describe the MIT near T_C. Recently, Vergés *et al.* [20] have shown that the carrier-lattice interaction leads to the MIT. The lattice polaron effect considered in Ref. [11] can also be taken in the same context. On the other hand, it is known that there exists considerable disorder due to Eu vacancies in EuB_6 samples [21]. In view of the negligible isotope effect reported for EuB_6 [8], the impurity effects might be more important than the lattice effects on the transport of EuB_6. We have thus examined the impurity effects on the magnetic and transport properties by incorporating the site-dependent impurity potential in the magnetic polaron model, as introduced in Eq. (1).

Figures 3(a) and 3(b) present the temperature dependent magnetization and resistivity when considering the attractive impurity potential of $\varepsilon_0 = -1.5$ [22]. Here we considered a system in the dilute limit ($n = 0.0156$) with $J_{AF} = 0$. The magnetization behavior does not change much from the case without disorder. In contrast, the transport property is modified dramatically. The resistivity now has a peak centered at $T_P = 0.07$, manifesting a feature of the MIT. The peak is thought to be caused by the formation of the so-called bound magnetic polaron. Indeed Fig. 3(c), which plots the averaged spin configuration at each temperature, clearly shows the magnetic polaron features around T_P. It is indicated that the insulating nature above T_P originates from the carrier localization by forming the bound magnetic polaron, while the metallic nature below T_p from the increasing size and resulting
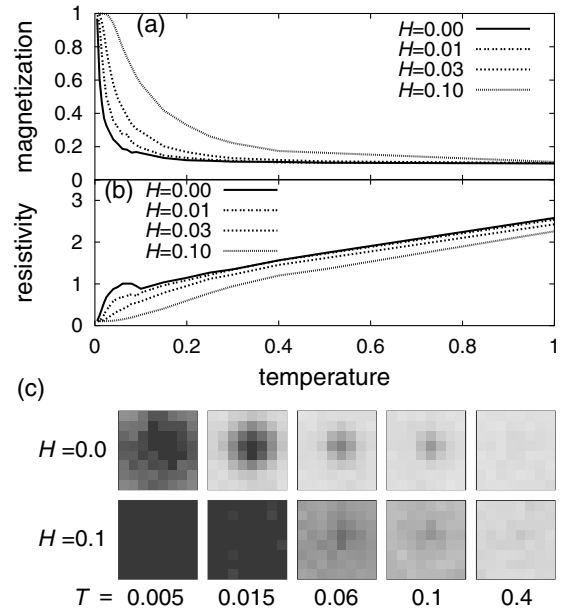
FIG. 3. (a) Magnetization and (b) resistivity in the presence of an impurity with an attractive potential of $\varepsilon_0 = -1.5$ in the dilute limit ($n = 0.0156$) ($J_{AF} = 0$). (c) The averaged spin configuration at each temperature with and without the external magnetic field. The magnetic polaron feature is evident for $H = 0$.

PHYSICAL REVIEW LETTERS
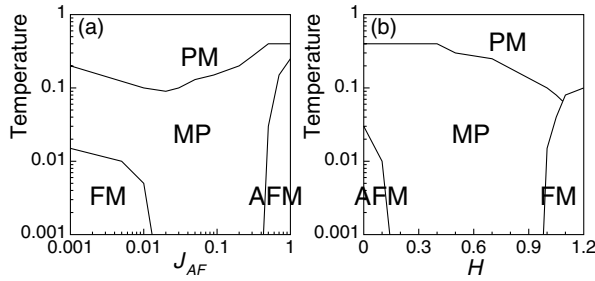
FIG. 4. (a) Schematic phase diagram of the FM Kondo lattice model ($J_H/t = 20$) with J_{AF} in the low density limit ($n = 0.0156$). PM and MP represent the paramagnetic and the magnetic-polaronic state, respectively. (b) The phase diagram with the external magnetic field for $J_{AF} = 0.5$.

overlap of magnetic polarons, as is consistent with the percolation concept. To our knowledge, this is the first theoretical demonstration of the magnetic polaron formation in the vicinity of the MIT. The MP state in this case is realized by FM clusters embedded in the paramagnetic background. Noteworthy is that the MIT temperature T_P is higher than the magnetic transition temperature T_C, which is consistent with the two-consecutive transition scenario [23]: the higher transition temperature corresponds to the metallization temperature, while the lower one to the magnetization temperature [24]. The resistivity shows a minimum at $T_M = 0.1$ and then increases upon heating, which is in good agreement with the observation for EuB$_6$. It is also seen in the bottom of Fig. 3(b) that, in the presence of the magnetic field, the resistivity peak is suppressed, and the negative MR is obtained near and above T_C. This behavior also agrees quite well with experiments. Accordingly, the magnetic polaron feature that appeared at $T_C < T < T_M$ for $H = 0$ is weakened for $H = 0.1$, resulting in more or less homogeneous spin configurations.

The phase diagrams in Fig. 4 summarize our results. With increasing J_{AF}, the ground state varies from the FM to the MP state, and eventually into the AFM state. Upon cooling, the FM and AFM states are preceded by the MP state which can be characterized by magnetic clusters and the peak or the hump structure in the resistivity curve. The impurity effect expands the MP region, but does not modify the gross form of the phase diagram. As shown in Fig. 4(b), the AFM ground state for large J_{AF} is easily broken by the magnetic field to become an MP state, and then to a FM state for the stronger field. Interestingly, if one changes the parameter J_{AF} by x of La concentration, Fig. 4 well describes the phase diagram of Eu$_{1-x}$La$_x$B$_6$. The preformed magnetic clustered state prior to the FM transition was already suggested in relation to the DMS system [25]. Although our discussions are focused on the explanation of the specific experimental results of Eu$_{1-x}$La$_x$B$_6$, the model and the results are very general and can be applied to any appropriate system which shows the MIT near T_C.

In conclusion, we have investigated the FM Kondo lattice model with the AFM interaction between local moments, and confirmed the existence of the magnetic polarons in the PS region in between the FM and AFM states in the phase diagram. The MP state is featured by FM clusters embedded in the AFM or the paramagnetic background and by the insulating behavior in the resistivity. The MP state can also be induced from the AFM state by applying the magnetic field, but the strong magnetic field drives it back to the FM state. The disordered impurity helps the magnetic polaron formation to produce the resistivity peak and the corresponding MIT for small J_{AF}. All results based on the magnetic polaron model are very consistent with experimental results of Eu$_{1-x}$La$_x$B$_6$.

[1] P.-G. de Gennes, Phys. Rev. **118**, 141 (1960).
[2] T. Dietl and J. Spalek, Phys. Rev. Lett. **48**, 355 (1982); A. Kaminski and S. Das Sarma, *ibid.* **88**, 247202 (2002).
[3] N. F. Mott, Contemp. Phys. **31**, 373 (1990).
[4] S. von Molnár, J. Supercond. **14**, 199 (2001).
[5] D. Heiman *et al.*, Phys. Rev. B **27**, 4848 (1983).
[6] J. M. de Teresa *et al.*, Nature (London) **386**, 256 (1997).
[7] P. Nyhus *et al.*, Phys. Rev. B **56**, 2717 (1997).
[8] C. S. Snow *et al.*, Phys. Rev. B **64**, 174412 (2001).
[9] H. Rho *et al.*, Phys. Rev. Lett. **88**, 127401 (2002).
[10] E. L. Nagaev, J. Magn. Magn. Mater. **110**, 39 (1992); P. Majumdar and P. Littlewood, Phys. Rev. Lett. **81**, 1314 (1998); H. Meskine *et al.*, *ibid.* **92**, 56 401 (2004).
[11] J. Chatterjee *et al.*, Phys. Rev. B **69**, 134423 (2004).
[12] J.-S. Rhyee *et al.*, Phys. Rev. B **65**, 205112 (2002).
[13] J.-S. Rhyee *et al.*, J. Appl. Phys. (to be published).
[14] N. Metropolis *et al.*, J. Chem. Phys. **21**, 1087 (1953).
[15] See, e.g., W. H. Press *et al.*, *Numerical Recipes in C* (Cambridge University Press, New York, 1992).
[16] E. R. Davidson, J. Comput. Phys. **17**, 87 (1975).
[17] S. Yunoki *et al.*, Phys. Rev. Lett. **80**, 845 (1998); S. Yunoki and A. Moreo, Phys. Rev. B **58**, 6403 (1998); H. Yi and J. Yu, *ibid.* **58**, 11 123 (1998).
[18] It is because of the second order AFM kinetic exchange interaction of $\sim t^2/J_H$.
[19] E. Dagotto, Rev. Mod. Phys. **66**, 763 (1994).
[20] J. A. Vergés *et al.*, Phys. Rev. Lett. **88**, 136401 (2002).
[21] Y. Isikawa *et al.*, Solid State Commun. **22**, 573 (1977); Z. Fisk *et al.*, J. Appl. Phys. **50**, 1911 (1979).
[22] The Eu vacancy will produce hole carriers and so they are attracted to an effectively negatively charged empty Eu site.
[23] S. Süllow *et al.*, Phys. Rev. B **62**, 11 626 (2000).
[24] The values of T_C and T_P are sensitive to the parameters used for the calculation. For example, for $J_H/t = 5$, the resulting T_C and T_P are 0.01 and 0.025, respectively.
[25] M. Mayr *et al.*, Phys. Rev. B **65**, 241202(R) (2002).